values reach very low-pressure values with peak locations moving downstream.

High-Lift Configuration

For the high-lift configuration the flaps were considered to be deflected 23 deg downward (landing mode). Solutions were obtained at $\alpha = 1$, 4, and 7.5 deg on a mesh having a total of 1,467,309 cells and 242,984 points, with 72,615 points on the aircraft surface. The surface grid is shown in Fig. 4. Figure 5 shows the pressure contours on the aircraft at $\alpha = 7.5$ deg. C_p distributions at various angles of attack are given at the 32% spanwise location in Fig. 6. It is clear that the freestream angle of attack has no significant effect on the pressure distribution on the surface of the flaps. Because at this relatively high flap deflection angle, flow over the flaps is insensitive to any change in the angle of attack.

Because no experimental data on the aircraft configuration studied were available in the open literature, the CFD results were compared with the results of Ref. 6 using the Advanced Aircraft Analysis Software. This software is based on the lifting-line theory and semiempirical formulations, which are commonly used in preliminary aircraft design.[7] As shown in Fig. 7, both of the methods show linear variations for all aerodynamic coefficients with angle of attack, having nearly the same slopes for C_M but slightly different slopes for C_L.

Computational Details

The aircraft solutions were obtained with approximately 1000 iterations for a residual reduction of about 1.5 orders of magnitude. Cruise configuration solutions of the aircraft took about one week for each angle of attack and required 1103 MB of memory on an HP-UX workstation. For the high-lift configuration solutions took about two weeks for each angle of attack and required 1275 MB of memory. It was observed that the memory requirement of the code was directly proportional to the number of cells in the computational domain.

In this work the Courant–Friedrichs–Lewy (CFL) number was varied from 1 to a final value of 100. However, when convergence problems were encountered the upper limit for the CFL number was reduced to 50 or 25. The explicit Runge–Kutta and point implicit schemes had convergence problems in all of the cases. For this reason a fully implicit scheme was used in all of the computations, although it required more computer memory.

Conclusions

Inviscid, subsonic flow solutions for a medium-range cargo aircraft were obtained on unstructured grids at cruise and high-lift configurations. From geometry modeling to the flow solution, this study was performed using the CFD-GEOM-V5 grid-generation code and the CFD-FASTRAN-V2.2 flow solver code.

The results showed that the lift coefficients varied linearly for the cruise and landing configurations. The pitching-moment coefficients showed the characteristics of a stable aircraft. Comparison of the CFD and the empirical solutions indicated a reasonable agreement for the lift and moment coefficients.

References

[1]Bahar, C., "Euler Solutions for a Medium Range Cargo Aircraft," M.S. Thesis, Dept. of Aerospace Engineering, Middle East Technical Univ., Ankara, Turkey, Jan. 2001.

[2]CFD-FASTRAN User Manual, Ver. 2.2, CFD Research Corp., Huntsville, AL, 1998.

[3]CFD-GEOM User Manual, Ver. 5, CFD Research Corp., Huntsville, AL, 1998.

[4]CFD-GEOM Tutorials, Ver. 5, CFD Research Corp., Huntsville, AL, 1998.

[5]Dodbcle, S. S., "Three Dimensional Aerodynamic Analysis of a High-Lift Transport Configuration," AIAA Applied Aerodynamic Conference, AIAA Paper 93-3536, Monterey, CA, Aug. 1993.

[6]Karaağaç, C., "The Aerodynamics, Flight Mechanics and Performance Predictions for a Medium Range Cargo Aircraft," M.S. Thesis, Dept. of Aerospace Engineering, Middle East Technical Univ., Ankara, Turkey, Nov. 1998.

[7]Roskam, J., *Airplane Design*, Roskam Aviation and Engineering Corp., Ottowa, KS, 1985.

Analytical Representation of Aerodynamic Forces in Laplace Domain

Bertil A. Winther*
The Boeing Company,
Huntington Beach, California 92647-2048

Nomenclature

$\boldsymbol{A}_k$	=	system matrix for model k
$\boldsymbol{C}$	=	general matrix $\boldsymbol{M}$ or $\boldsymbol{P}$
D	=	determinant of dynamic system
E_i	=	aerodynamic coefficients due to pitch
h	=	vertical position coordinate
$\boldsymbol{I}$	=	identity matrix
ℓ	=	reference length
$\boldsymbol{M}$	=	mass matrix
N_n	=	numerator terms in response equation
$\boldsymbol{P}$	=	complex aerodynamic force matrix
p_j	=	aerodynamic pressure on surface
$\boldsymbol{Q}$	=	aerodynamic force matrix in Laplace domain
q	=	pitch rate at c.g.
S	=	area of surface exposed to airflow
s	=	Laplace variable
t	=	time
U	=	mean velocity of airflow
w	=	downwash on aircraft surface
$\boldsymbol{X}_k$	=	state-variable vector for model k
x, y, z	=	aircraft mean-flight-path axes
α	=	angle of attack at c.g.
Δn_z	=	incremental load factor at c.g.
δ	=	control surface deflection
ζ	=	displacement in z direction
θ	=	pitch angle
λ	=	complex eigenvalue
μ	=	structural mass density
τ	=	reference time
Φ_j	=	shape of mode j
ω	=	circular frequency

Subscripts

h	=	control surface hinge value
i, j	=	modal indices
s	=	steady-state value
0	=	value at aircraft c.g.

Superscript

T	=	transposed matrix

Introduction

TO predict aeroelastic stability and response, the equations of motion (EOM) normally are formulated in the frequency domain. In accordance with the small-displacement theory, a linear

Received 20 December 2001; revision received 6 October 2002; accepted for publication 18 November 2002.

*Senior Principal Engineer, Phantom Works, Loads, and Dynamics.

combination of rigid-body modes and a suitable number of natural-vibration modes are used to describe structural deformations caused by inertial, aerodynamic, and elastic forces. The oscillatory aerodynamic forces consist of in-phase and out-of-phase components that are represented by complex coefficients evaluated by assuming constant harmonic motion at discrete frequencies. Therefore, these coefficients do not include the effect of damped motion and depend only on frequency and Mach number.

To account for the time–history effect, it is customary to define analytical continuations that satisfy certain boundary conditions in the Laplace domain. Various analytical representations and their effect on the predicted response are addressed in the following sections. As expected, the differences are usually small and may be significant only for modes with a high level of aerodynamic damping, for example, the short-period mode. Nevertheless, the phenomena may be of some interest to students of flight mechanics. More useful to practicing engineers are equations for the steady-state response limits, that is, angle of attack, pitch rate and load factor, that are derived as part of the current investigation.

Design of advanced flight control systems involves piloted (real-time) simulations as well as frequency-domain analyses. When the structural dynamic characteristics of the aircraft are considered, the EOM used in flight simulations become identical in principle to the ones solved in flutter analyses. Traditionally, flutter analysts are concerned mainly with the natural-vibration modes because the rigid-body modes normally are highly damped and well separated in frequency from the structural response. The rigid-body dynamics, however, may be important in flutter investigations of large flexible aircraft (where the fundamental vibration frequency is close to the short-period frequency) or in aeroservoelastic analyses of control-configured vehicles that employ high-gain flight control systems.

To facilitate time-domain solutions and to streamline the design process in flight controls engineering, the equations are transferred into a state-variable form with time-invariant coefficients. Techniques to transfer the flutter equations from the frequency domain to the time domain have been researched for many years, and several approximate methods are now available. The approach presented in Ref. 1 (often referred to as the P-transform process) may be described as a minimum-state approximation that in many cases eliminates the need for auxiliary variables to represent aerodynamic phase lags.

In applications of the method, however, eigenvalues associated with the short-period oscillation were observed to be slightly different than those obtained in the flutter solution. It was suggested in Ref. 1 that the results were caused by poor numerical convergence of the mean-flight-path (MFP) axis formulation commonly used in flutter analyses. Further investigation showed this explanation to be incorrect, and it was demonstrated that the discrepancy is caused by differences in the aerodynamic force representation described in the present Engineering Note.

Analytical Continuation

To illustrate the concept of analytical continuation for aerodynamic forces in the Laplace domain, it is sufficient to consider the relatively simple problem of an aircraft in horizontal flight with two degrees of freedom, plunge and pitch. In the initial discussion, perturbations relative to the mean flight path will be described in a coordinate system x, y, z that moves with the average velocity of the aircraft. This type of reference frame differs from the body-axis system used by flight control engineers, but it is the conventional one in flutter analysis. For lack of a better name we will refer to it as the MFP-axis system. It is defined as having the x axis pointing forward, y axis positive on the starboard side, and the z axis positive down. Vertical perturbations of the aircraft then may be described in the time domain by

$$\zeta = \Phi_1(x, y)h(t) + \Phi_2(x, y)\theta(t) \tag{1}$$

The plunge and pitch displacements are defined by

$$\Phi_1 = \ell, \qquad \Phi_2 = x_0 - x \tag{2}$$

Inertial and aerodynamic generalized forces of mode $[i]$ caused by a perturbation in mode $[j]$ then may be written in the following form:

$$M_{ij} = \int \mu \Phi_i \Phi_j \, \mathrm{d}V, \qquad P_{ij}(\omega) = \int \Phi_i p_j \, \mathrm{d}S \tag{3}$$

As discussed in the preceding section, the aerodynamic forces are computed in the frequency domain by using the assumption of constant harmonic motion. Complex notation is introduced to separate each force into a real part that moves in phase with the displacement and an imaginary part that is in phase with the rate of displacement. The imaginary parts of the forces go to zero as the frequency approaches zero, but, for general oscillatory motion, a surface displacement contributes both to the real and to the imaginary component. To satisfy different requirements on accuracy and cost, there are a great many numerical methods that predict unsteady aerodynamic loads in various flight regimes. Based on the linear potential-flow theory, the doublet-lattice method[2,3] is the standard computational tool for the subsonic regime. In this method, real and imaginary parts of the oscillatory pressure acting on the aircraft are determined by the surface boundary condition:

$$w(x, y) = \frac{\partial \zeta}{\partial t} - U\frac{\partial \zeta}{\partial x} \tag{4}$$

Flutter stability is computed in an iterative manner by solving for the eigenvalues of the complex EOM. A true (converged) root is obtained when the imaginary part of an eigenvalue matches the assumed frequency of the aerodynamic forces. The estimated damping ratio (or alternately, the estimated structural damping value required for stability) is computed by taking the ratio of the real part and the magnitude of the root. By the use of the principle of analytical continuation for the aerodynamic forces, it has been determined that these estimates are valid within a narrow band of the imaginary axis, that is, for small damping ratios.

The same principle is used when the flutter equations are transferred from the frequency domain to the time domain. The simplest analytical continuations in the Laplace domain are described by

$$Q_{ij}(s) = Q_{ij}^{(0)} + sQ_{ij}^{(1)} + s^2 Q_{ij}^{(2)}$$

$$Q_{ij}^{(0)} = \mathrm{Re}(P_{ij}), \qquad Q_{ij}^{(1)} = \mathrm{Im}(P_{ij})/\omega, \qquad Q_{ij}^{(2)} = 0 \tag{5}$$

In the following discussion, this representation is referred to as model a. To distinguish the forces P for constant harmonic motion from the corresponding ones in the Laplace domain, the latter are represented by Q. The boundary condition here is imposed in the frequency domain at a point on the imaginary axis, that is, ω axis, where the generalized force is known. It is observed that in the steady-state limit, that is, $\omega = 0$, all forces caused by the plunge degree of freedom vanish. This may be exploited by imposing additional boundary conditions for the following terms:

$$Q_{i1}^{(0)} = 0, \qquad Q_{i1}^{(2)} = -\mathrm{Re}(P_{i1})\big/\omega^2 \tag{6}$$

The modification of model a is model b. Sometimes $Q_{11}^{(2)}$ is called aerodynamic mass because it in effect is equivalent to an increase of the aircraft mass. It is proportional to the $C_{z\dot{\alpha}}$ coefficient that appears in the EOM derived by Etkin.[4]

When the EOM are converted from the MFP-axis system to a body-axes system, as discussed in the next section, the following θ-induced forces appear:

$$E_i = Q_{i1}^{(1)} - \tau Q_{i2}^{(0)}, \qquad \tau = \ell/U \tag{7}$$

At the steady-state limit, the two elements forming these coefficients cancel each other. In the vertical force case, for instance, each one of the two terms, $Q_{11}^{(1)}$ and $Q_{12}^{(0)}$, has a limit value proportional to $C_{z\alpha}$. By imposing the steady-state boundary condition, one obtains

$$E_i = E_i^{(0)} + s^2 E_i^{(2)}, \qquad E_i^{(0)} = 0, \qquad E_i^{(2)} = -E_i(\omega)\big/\omega^2 \tag{8}$$

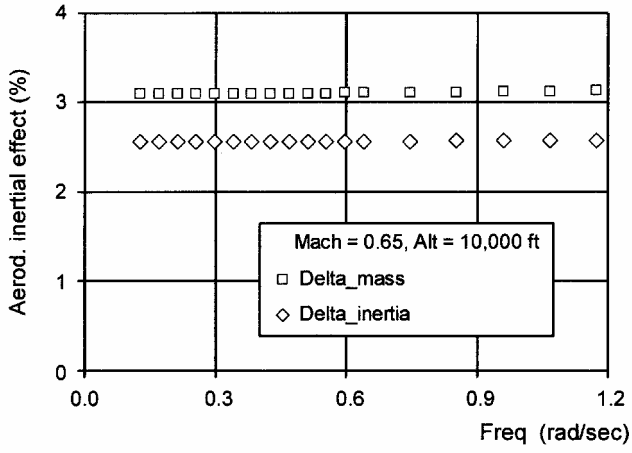

Fig. 1 Relative increases in apparent aircraft mass and moment of inertia.

This modification of model b is model c. The $E_2^{(2)}$ term may be referred to as aerodynamic inertia because it increases the effective mass moment of inertia. Etkin[4] considers it a second-order effect and neglects the term in his linear EOM.

To verify the validity of the analytical continuations, aerodynamic mass and inertia terms defined by Eqs. (6) and (8) were evaluated for an advanced transport configuration. Increases in apparent mass and mass moment of inertia due to the aerodynamics are shown in Fig. 1. As expected, these terms are practically invariant in the frequency range of interest for the short-period response.

EOM

Dynamic stability of the longitudinal rigid-body motion is governed by the equation:

$$\boldsymbol{M}\ddot{X}_1 - \boldsymbol{Q}^{(1)}\dot{\boldsymbol{X}}_1 - \boldsymbol{Q}^{(0)}\boldsymbol{X}_1 = 0 \tag{9}$$

The state-variable vector is defined by

$$\boldsymbol{X}_1 = [h \quad \theta]^T \tag{10}$$

Matrices $\boldsymbol{Q}^{(0)}$ and $\boldsymbol{Q}^{(1)}$ were introduced in Eq. (5). For the sake of simplicity the EOM may be transformed to the aircraft c.g. so that the mass matrix $\boldsymbol{M}$ contains only the diagonal elements $M_{11} = \ell^2 m$ and $M_{22} = I_y$, where m is aircraft mass and I_y the mass moment of inertia. Coordinates h and θ are nondimensional variables that are defined positive in the directions of the z and y axes, respectively. The system roots are obtained by solving for the eigenvalues of $\boldsymbol{A}_1$:

$$\boldsymbol{A}_1 = \begin{bmatrix} \boldsymbol{M}^{-1}\boldsymbol{Q}^{(1)} & \boldsymbol{M}^{-1}\boldsymbol{Q}^{(0)} \\ \boldsymbol{I} & 0 \end{bmatrix} \tag{11}$$

These roots are based on the analytical continuations of model (a) described in the preceding section. Model b is a natural consequence of the transformation from MFP axes (coordinates h and θ) to body axes (coordinates α and θ). The angle of attack at the c.g. is defined by

$$\alpha = w(x_0, t)/U \tag{12}$$

Equation (4) yields the relationship

$$\dot{h} = (\alpha - \theta)/\tau \tag{13}$$

By combining this equation with Eq. (8) and the model (b) representation of Eq. (5), one obtains

$$\bar{\boldsymbol{M}}\dot{X}_2 - \bar{\boldsymbol{Q}}X_2 = 0, \qquad X_2 = [\alpha \quad q \quad \theta]^T \tag{14}$$

The variable transformation causes the inclusion of aerodynamic coefficients in the modified mass matrix $\bar{\boldsymbol{M}}$. Similarly, the $\bar{\boldsymbol{Q}}$ matrix gets a contribution from the aircraft mass as follows:

$$\bar{\boldsymbol{M}} = \begin{bmatrix} \bar{M}_{11} & 0 & 0 \\ -Q_{21}^{(2)} & \tau M_{22} & 0 \\ 0 & 0 & 1 \end{bmatrix}, \qquad \bar{M}_{11} = M_{11} - Q_{11}^{(2)} \tag{15}$$

$$\bar{\boldsymbol{Q}} = \begin{bmatrix} Q_{11}^{(1)} & \tau Q_{12}^{(1)} + \bar{M}_{11} & -E_1 \\ Q_{21}^{(1)} & \tau Q_{22}^{(1)} - Q_{21}^{(2)} & -E_2 \\ 0 & 1 & 0 \end{bmatrix} \tag{16}$$

The quantities E_1, E_2, and τ are defined by Eq. (7) in the preceding section, where it was observed that the θ-dependent forces E_i vanish at the zero-frequency limit. This characteristic is the source of confusion for flutter analysts who are accustomed to linking the MFP-axis variable θ with α. In the body-axis system, however, angle of attack and pitch rate are independent motion variables (like $\dot{h}$ and $\dot{\theta}$ are in the MFP system).

Roots of the modified EOM are obtained by solving for the eigenvalues of $\boldsymbol{A}_2$:

$$\boldsymbol{A}_2 = (\bar{\boldsymbol{M}})^{-1}\bar{\boldsymbol{Q}} \tag{17}$$

By the use of relationships documented in Ref. 5, the aerodynamic forces of Eq. (14) may be expressed in terms of stability derivatives. Except for the E_i coefficients, the equations translate directly into Etkin's[4] linear formulation. For model b, these coefficients vanish at the steady-state limit. For model c, however, they are converted into apparent inertia terms based on the analytical continuation of Eq. (8). The EOM for model c are written as follows:

$$\tilde{\boldsymbol{M}}\dot{X}_3 - \tilde{\boldsymbol{Q}}X_3 = 0 \tag{18}$$

The quantities in this formulation are defined by

$$X_3 = [\alpha \quad q]^T, \qquad \tilde{\boldsymbol{M}} = \begin{bmatrix} \bar{M}_{11} & E_1^{(2)} \\ \bar{M}_{21} & \bar{M}_{22} \end{bmatrix}$$

$$\tilde{M}_{22} = \bar{M}_{22} + E_{22}^{(2)}, \qquad \tilde{\boldsymbol{Q}} = \begin{bmatrix} \bar{Q}_{11} & \bar{Q}_{12} \\ \bar{Q}_{21} & \bar{Q}_{22} \end{bmatrix} \tag{19}$$

The model c stability characteristics are determined by the eigenvalues of $\boldsymbol{A}_3$:

$$\boldsymbol{A}_3 = (\tilde{\boldsymbol{M}})^{-1}\tilde{\boldsymbol{Q}} \tag{20}$$

Steady-State Limits

For evaluation of the response caused by pilot inputs, the generalized forces due to a control surface motion need to be introduced. The displacement on the surface is defined by

$$\zeta_3 = (x - x_h)\delta(t) \tag{21}$$

The dynamic responses caused by control inputs are

$$h/\delta = (\hat{M}_{22}\hat{Q}_{13} + Q_{12}\hat{Q}_{23})/D$$

$$\theta/\delta = (\hat{M}_{11}\hat{Q}_{23} + Q_{21}\hat{Q}_{13})/D \tag{22}$$

Coefficients appearing in Eq. (22) are defined by

$$\hat{M}_{jj} = s^2 M_{jj} - Q_{jj}, \qquad \hat{Q}_{j3} = Q_{j3} - s^2 M_{j3}$$

$$D = \hat{M}_{11}\hat{M}_{22} - Q_{12}Q_{21} \tag{23}$$

As the frequency goes to zero, the following quasi-steady limits are obtained:

$$\frac{\ddot{h}_s}{\delta} = \lim_{s\to 0}\frac{N_1 + s(N_2 - N_3)}{D_s}, \qquad \frac{q_s}{\delta} = \lim_{s\to 0}\frac{N_4 - sN_5}{D_s} \tag{24}$$

The numerator and the denominator terms are defined as follows:

$$N_1 = Q_{22}^{(0)} Q_{13}^{(0)} - Q_{12}^{(0)} Q_{23}^{(0)}, \qquad N_2 = Q_{22}^{(1)} Q_{13}^{(0)} + Q_{22}^{(0)} Q_{13}^{(1)}$$

$$N_3 = Q_{12}^{(1)} Q_{23}^{(0)} + Q_{12}^{(0)} Q_{23}^{(1)}, \qquad N_4 = Q_{11}^{(1)} Q_{23}^{(0)} - Q_{21}^{(1)} Q_{13}^{(0)}$$

$$N_5 = \left(M_{11} - Q_{11}^{(2)}\right) Q_{23}^{(0)} + Q_{21}^{(2)} Q_{13}^{(0)}, \qquad D_s = D_1 + D_2$$

$$D_1 = \left(M_{11} - Q_{11}^{(2)}\right) Q_{22}^{(0)} + Q_{21}^{(2)} Q_{12}^{(0)}$$

$$D_2 = Q_{21}^{(1)} Q_{12}^{(1)} - Q_{11}^{(1)} Q_{22}^{(1)} \tag{25}$$

It is necessary to carry the first-order as well as the zero-order coefficients in Eq. (24). When Eq. (13) is applied for calculation of the steady-state angle of attack, one finds that the terms N_1/s and N_4/s cancel each other thereby yielding a finite value for α_s as follows:

$$\frac{\alpha_s}{\delta} = \frac{-N_5 + \tau(N_2 - N_3)}{D_s} \tag{26}$$

As expected, $(\dot{h}/\delta)$ and (θ/δ) have no steady-state limits. The limits for load factor Δn_{zs} and pitch rate q_s are

$$\Delta n_{zs}/\delta = -N_1 \ell / g D_s, \qquad q_s/\delta = N_4/D_s \tag{27}$$

We observe that none of these steady-state limits include pitch acceleration coefficients (neither inertial nor aerodynamic). This result validates Etkin's[4] quasi-steady assumption discussed in connection with the formulation of Eq. (8).

Numerical Applications

Differences between the three aerodynamic models were evaluated numerically by using the preliminary design of a commercial transport aircraft. The chosen configuration is statically stable when the structural flexibility is considered but, for the simplified EOM presented here, that is, limited to rigid-body degrees of freedom, the solution would reflect the characteristics of an aircraft that is only marginally stable in the static sense. Therefore, to make the present application more realistic, the c.g. was moved forward by 2.8% of the mean-aerodynamic-chord length.

In this context, note that, at the cost of more cumbersome formulations, the EOM presented could be augmented by additional degrees of freedom to account for flexibility as well as structural dynamic effects. The quasi-steady effect of elastic deformations may in fact be considered simply by replacing rigid-body force coefficients with "residualized" terms using the technique described in Ref. 1 and elsewhere.

The EOMs were transformed to the new pitch axis, that is, to the relocated c.g., by performing the following operation on the mass and aerodynamic matrices:

$$\boldsymbol{C}_{\text{new}} = \boldsymbol{T}\boldsymbol{C}_{\text{old}}\boldsymbol{T}^T, \qquad \boldsymbol{T} = \begin{bmatrix} 1 & 0 \\ -M_{21}/M_{11} & 1 \end{bmatrix} \tag{28}$$

The doublet-lattice method[2,3] was applied to generate aerodynamic force coefficients for a large number of ω values. At chosen frequencies, the short-period roots λ were computed for each of the three models discussed earlier. Results for the imaginary parts of the eigenvalues are presented in Fig. 2 with a dotted line showing the locus of converged solutions, that is, where the imaginary part matches the frequency. As expected, the short-period roots associated with models a and c are seen to be practically invariant in the frequency range of interest. Also, it is observed that the model a and the model b frequencies are nearly equal at the point of convergence, that is, 0.56 rad/s. The short-period frequency for model c, however, is about 28% lower, that is, 0.40 rad/s. For evaluation of Etkin's[4] approximation, an additional computation was performed without the aerodynamic pitch acceleration term in model c. The converged frequency (not shown in Fig. 2) is virtually the same, 0.41 rad/s. For each model, the damping in the short-period mode was obtained by computing the ratio of the real part and the magnitude of the eigenvalue at the frequencies of convergence. These ratios are all relatively close, 83% for model a, 87% for model b, and 89% for model c. Etkin's approximation, a modification of model c, yields a damping ratio of 89%.

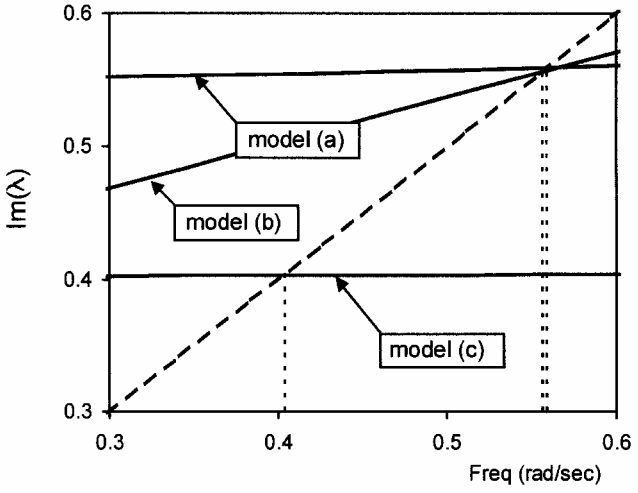

Fig. 2 Imaginary parts of eigenvalues vs frequency for each model.

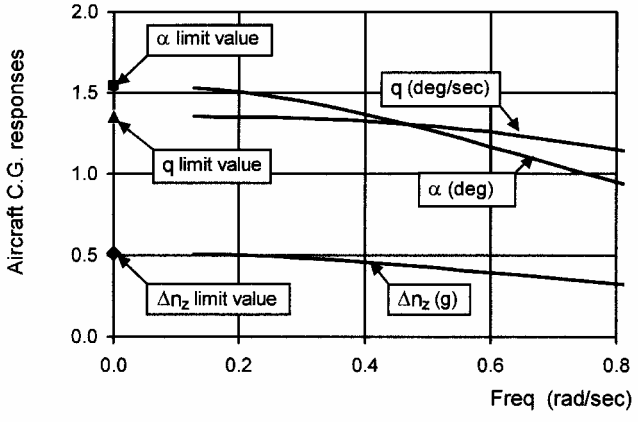

Fig. 3 Aircraft responses at center of gravity per degree of elevator deflection.

As a consequence of singularities in the EOM, there are additional (nonconverged) eigenvalues for model a and model b near the origin, $\omega = 0$. In model c, all numerical difficulties are eliminated because its solution has only one pair of roots. Therefore, it is postulated that this model yields a more accurate description of the aircraft dynamics at low frequencies. Currently the P-transform process[1] is implemented with model c as the preferred option.

The frequency-response functions, as well as the limit values derived in the preceding section, are by definition evaluated on the frequency axis where all three of the analytical models are equal. Results for incremental load factor, pitch rate, and angle of attack are presented in Fig. 3. It is observed that the limit value for the angle of attack is finite even though, as discussed in connection with Eq. (26), it consists of a combination of the unbounded components $\dot{h}$ and θ.

Conclusions

With the impetus provided by numerical differences between the body-axis solution and the flutter (MFP-axis) solution for the short-period response, the current study was undertaken to gain a better understanding of the aerodynamic force models. The difference in the low-frequency response was inaccurately explained in Ref. 1 as a numerical convergence problem intrinsic to the MFP-axis formulation. Further investigation showed that the discrepancy rather is a consequence of differing aerodynamic force representations in the Laplace domain. In the present Engineering Note, various aerodynamic models, that is, analytical continuations related to the

choice of reference system, are described. It is demonstrated how the MFP-axis formulation introduces singularities in the EOM. The singularities are identified, and the effect of their removal is shown in a numerical application. The conclusion is that the body-axis formulation generally leads to a more accurate solution.

As part of the current investigation, equations were derived for the steady-state limits of common motion variables. These limits are not affected by the various modeling techniques discussed here.

Acknowledgment

The author wishes to thank Daniel M. Ortega of the Boeing Phantom Works, Department of Loads and Dynamics, for generating the structural and aerodynamic data that were used in the sample problem.

References

[1]Winther, B. A., Goggin, P. J., and Dykman, J. R., "Reduced-Order Aeroelastic Model Development and Integration with Nonlinear Simulation," *Journal of Aircraft*, Vol. 37, No. 5, 2000, pp. 833–839.

[2]Albano, E., and Rodden, W. P., "A Doublet-Lattice Method for Calculating Lift Distributions on Oscillating Surfaces in Subsonic Flow," *AIAA Journal*, Vol. 7, No. 2, 1969, pp. 279–285.

[3]Giesing, J. P., Kalman, T. P., and Rodden, W. P., "Subsonic Unsteady Aerodynamics for General Configurations," U.S. Air Force Flight Dynamics Lab., Rept AFFDL-TR-71-5, Dayton, OH, Nov. 1971.

[4]Etkin, B., *Dynamics of Flight*, Wiley, New York, 1959, pp. 189–225.

[5]Rodden, W. P. (ed.), *MSC/NASTRAN Handbook for Aeroelastic Analysis*, MSR-57, MacNeal–Schwendler, Los Angeles, CA, Nov. 1987, Chaps. 8–10.

Extending Slender Wing Theory to Not So Slender Wings

Lance W. Traub*
Texas A&M University,
College Station, Texas 77843-3141

Nomenclature

AR	=	aspect ratio
a.c.	=	aerodynamic center
b	=	wing span
$b(x)$	=	local wing span
C_{Di}	=	induced drag coefficient
C_L	=	lift coefficient
$C_{L\alpha}$	=	lift-curve slope
$C_l(x)$	=	local lift coefficient
$Cm_{\text{l.e.}}$	=	wing apex pitching moment coefficient
Cr	=	root chord
C_T	=	leading-edge thrust coefficient
Kv	=	vortex lift constant
L	=	lift
$m(x)$	=	local apparent mass
S	=	wing area
U	=	freestream velocity
x, y	=	Cartesian coordinate
x_{cl}	=	location of wing's center of lift
α	=	angle of attack
α_i	=	induced angle of attack
ε	=	wing apex half angle
Λ	=	wing leading-edge sweep angle
ρ	=	density

Received 13 June 2002; revision received 16 October 2002; accepted for publication 18 October 2002.

*Texas Engineering Experiment Station Research Scientist/Lecturer, Aerospace Engineering Department. Associate Member AIAA.

Introduction

THE delta wing configuration has been extensively studied as a configuration that represents a realistic compromise between high-speed efficiency and low-speed maneuverability. The widespread adoption of this configuration in the late 1940s and 1950s promulgated the development of theoretical methods capable of predicting the behavior of these wings. Non-numerical efforts to predict the attached flow lift included slender wing theory (SWT)[1,2] and the method of Lawrence.[3] SWT was further developed by Lomax and Sluder[4] to account for the trailing-edge Kutta condition and compressibility. The resulting expressions compare reasonably with experiment[4] but are somewhat cumbersome, lacking the simplicity and ease of computation inherent in the original formulation. Similar observations can be made regarding the method of Lawrence.[3]

SWT[1,2] yields simple expressions to predict the lift, drag, and pitching moment coefficient of slender delta wings with fully attached leading-edge flow. However, the simplifications inherent in SWT limit its utility for wings with aspect ratios generally greater then 0.5, due to preclusion of trailing-edge effects. It is assumed that the chordwise velocity gradients are negligible such that the governing linearized partial differential equation transforms to Laplace's equation in a crossflow plane. Wing properties are evaluated in this cross flowplane that is assumed representative for all crossflow planes. As the wing extends to infinity chordwise, each crossflow plane is essentially a Trefftz plane. SWT predicts an elliptic spanwise load distribution. As chordwise effects are neglected in this methodology, the results are applicable for incompressible and compressible flow. The primary results from SWT are summarized as follows:

$$C_{L\alpha} = (\pi/2)\text{AR}, \qquad C_{Di} = C_L^2 \big/ \pi\,\text{AR} = (\pi/4)\text{AR}\alpha^2$$

$$\text{a.c.}/Cr = \tfrac{2}{3}, \qquad Cm_{\text{l.e.}} = -\pi\,\text{AR}\alpha/3$$

The simplicity of these equations makes them attractive for preliminary design use, as well as for educational purposes, as they can readily be committed to memory. However, their poor accuracy for the majority of practical delta wing configurations limits their utility. It would be useful for these applications to have similarly simple expressions that are applicable to a wider range of delta wings. In this Note, SWT is extended to include trailing-edge effects. Resulting expressions are compared with numerical and experimental data for validation.

Methodology

In the following analysis, it is assumed that the delta wings are planar and that their leading-edge flow is fully attached (100% leading-edge suction). The fluid is also assumed incompressible. Jones'[1] presentation of SWT relates the lift per unit chord of the wing to the rate of increase of the apparent mass of the fluid in a fixed axial crossflow plane as its penetrated by the wing. As the wing penetrates the plane, the scale of the flow increases, requiring a lift force equal to the downward velocity multiplied by the local increase of the additional apparent mass.[1] At any crossflow plane, the apparent mass of the fluid is given by

$$m(x) = \rho\pi b(x)^2/4 \tag{1}$$

Equation (1) represents the apparent mass for a falling flat plate, showing that the local fluid entrained consists of a cylinder with a diameter equal to that of the local wingspan. Consequently, $m(x)$ increases parabolically toward the trailing edge of the wing. The lift per unit chord is related to the apparent mass by [noting that $b(x) = 2x\tan(\varepsilon)$]

$$\frac{\mathrm{d}L}{\mathrm{d}x} = U^2\alpha\frac{\mathrm{d}m(x)}{\mathrm{d}x} = U^2\alpha\rho\pi\frac{2b(x)}{4}\frac{\mathrm{d}b(x)}{\mathrm{d}x} = U^2\alpha\rho 2\pi x\tan(\varepsilon)^2 \tag{2}$$

As such, the rate of change of the apparent mass and, hence, local lift varies linearly with chordwise distance. Equation (2) implies that if